

Development of a recombinant single-cycle influenza viral vector as an intranasal vaccine against SARS-CoV-2

Received: 21 December 2025

Accepted: 25 May 2026

Published online: 13 June 2026

Cite this article as: Munro J., Melnyk D., Afzal M. *et al.* Development of a recombinant single-cycle influenza viral vector as an intranasal vaccine against SARS-CoV-2. *Sci Rep* (2026). <https://doi.org/10.1038/s41598-026-55581-y>

Jonathan Munro, Diana Melnyk, Madeeha Afzal, Lisa Schimanski, Alexander A. Cohen, Jennifer R. Keefe, Pamela J. Bjorkman, William S. James, Alain R. Townsend & Tiong Kit Tan

We are providing an unedited version of this manuscript to give early access to its findings. Before final publication, the manuscript will undergo further editing. Please note there may be errors present which affect the content, and all legal disclaimers apply.

If this paper is publishing under a Transparent Peer Review model then Peer Review reports will publish with the final article.

Development of a Recombinant Single-Cycle Influenza Viral Vector as an Intranasal Vaccine against SARS-CoV-2

Jonathan Munro¹, Diana Melnyk¹, Madeeha Afzal², Lisa Schimanski¹, Alexander A. Cohen⁴, Jennifer R. Keeffe⁴, Pamela J. Bjorkman⁴, William S. James², Alain R. Townsend^{1,3}, Tiong Kit Tan^{1,3}

¹ MRC Translational Immune Discovery Unit, Weatherall Institute of Molecular Medicine University of Oxford, Oxford OX3 9DS, UK.

² Sir William Dunn School of Pathology, University of Oxford, Oxford OX1 3RE, UK.

³ Chinese Academy of Medical Sciences-Oxford Institute, Nuffield Department of Medicine, University of Oxford, Oxford OX3 7FZ, UK.

⁴ Division of Biology and Biological Engineering, California Institute of Technology, Pasadena, CA 91125, USA.

* Correspondence:

Corresponding Authors

Tiong Kit Tan, jack.tan@ndm.ox.ac.uk,

Alain Townsend, alain.townsend@imm.ox.ac.uk

Keywords: non-replicating viral vector, influenza, SARS-CoV-2, vaccine

Abstract

The COVID-19 pandemic has demonstrated the detrimental potential of zoonotic coronavirus transmission to human populations. Effective vaccines capable of eliciting immunity to SARS-CoV-2 have been pivotal in mitigating the spread of the virus. In this study, we describe the generation of a non-replicating pseudotyped influenza A virus (S-FLU), where the native haemagglutinin (HA) sequence is replaced with the coding sequence of either a membrane-anchored form (TM) or secretory form (Sec) of the receptor-binding domain (RBD) of the ancestral SARS-CoV-2 Wuhan (S-RBD Wuhan). We showed that both S-RBD-TM and S-RBD-Sec viruses can be generated via reverse genetics and grown to high titre. Intranasal immunisation in mice with S-RBD-TM elicits robust serum binding and neutralisation activity against SARS-CoV-2,

superior to S-RBD-Sec. Furthermore, we demonstrate that a heterologous prime-boost immunisation regimen in mice with S-RBD-TM Wuhan and S-RBD-TM BM48-31 (a distant Clade 3 SARS-like betacoronavirus (sarbecovirus)) increases antibody binding breadth against mismatched sarbecoviruses compared to homologous prime-boost with S-RBD-TM Wuhan, although this did not translate into significantly enhanced cross-neutralisation across the tested virus panel. These results demonstrate that S-RBD delivery via the intranasal route induces both systemic and mucosal antibody responses and provide a foundation for further optimisation of S-RBD sarbecovirus vaccine strategies.

Introduction

The global pandemic of 2020 was triggered by the emergence of SARS-CoV-2, a zoonotic SARS-like betacoronavirus (sarbecovirus) responsible for the respiratory disease COVID-19 [1, 2]. SARS-CoV-2 caused over 6 million reported deaths, with estimates of the true toll reaching 17.2 million [3]. Whilst vaccines have proven successful in reducing morbidity and mortality, several variants of concern (VOCs) have emerged, exhibiting increased transmissibility, disease severity, and immune evasion [4-8], posing challenges to vaccine efficacy [9-12].

Prior to SARS-CoV-2, six members of the *Coronaviridae* family spilled over to humans from animal reservoirs [13-17]. While four are endemic and cause non-severe symptoms [13], SARS-CoV-1 and MERS-CoV caused high mortality and morbidity [18-20]. Instances of simultaneous infection with SARS-CoV-2 and MERS-CoV in humans in the Middle East have been reported [21], with both viruses infecting type-II alveolar cells and utilising identical transcription regulatory sequences [1, 22]. Furthermore, the identification of numerous coronaviruses in bats, civets, and pangolins that share similar genomes with SARS-CoV-2 and utilise the human ACE2 as a host cell receptor highlights their potential to spill over into humans [2, 15, 23]. Therefore, there is great concern and apprehension regarding the potential for future zoonotic coronavirus spillover events that could precipitate new pandemics [24-27]. This highlights the importance of being proactive rather than reactive, by developing broader spectrum sarbecovirus vaccines to control the spread of SARS-CoV-2 variants and to prevent future pandemics from novel zoonotic sarbecoviruses [28, 29].

The sarbecovirus spike (S) glycoprotein consists of S1 and S2 subunits [30]. The S1 subunit is responsible for initial contact with host receptors [31] and contains the receptor-binding domain (RBD), which is highly immunogenic and the site recognised by most neutralising antibodies [32-35]. Structural studies have defined multiple classes of SARS-CoV-2 RBD-targeting antibodies based on their epitope location and angle of approach. Class 1 and 2 epitopes overlap the ACE2 binding interface, and antibodies targeting these regions typically neutralise by directly blocking receptor engagement. However, because the ACE2 interface is subject to frequent mutation, Class 1 and 2 antibodies are often strain specific. In contrast, Class 3 epitopes are located distal from the ACE2 interface and are generally more conserved across sarbecoviruses. Class 3 antibodies can mediate neutralisation through steric hindrance or Fc-dependent functions. Class 4 epitopes are also distal from the ACE interface, and tend to be highly conserved, although antibodies targeting the Class 4 epitopes are generally weakly neutralising. A subset of antibodies recognising overlapping Class 1/4 epitopes can exhibit both potent neutralisation and broad sarbecovirus reactivity. More recently, Class 5 epitopes have been described, comprising cryptic regions that are accessible when the RBD adopts specific conformations. Class 5 antibodies display broad sarbecovirus cross-reactivity, although their neutralising potency may vary [36-43].

We describe in this study the use of a modified single-cycle influenza virus vaccine (S-FLU), shown previously to have produced broad protection against influenza [44, 45], as a potential vaccine against SARS-CoV-2 and other zoonotic sarbecoviruses. Although similar approaches have been previously reported [46-49], S-FLU offers a key advantage as it can be pseudotyped safely with avian haemagglutinin subtypes (e.g., H5 or H7) for which there is minimal pre-existing immunity in the human population, thereby reducing the risk of immune interference with vaccine efficacy. Inactivation of the native haemagglutinin (HA) signal sequence means that S-FLU can only replicate in cell lines transfected to express HA that provide the surface protein for budding viral particles [45]. Briefly, we replaced the native HA coding sequence within the HA viral RNA (vRNA) with either a membrane-anchored form of the SARS-CoV-2 Spike RBD (S-RBD-TM) or a secreted form (S-RBD-Sec), based on the

prototypic Wuhan SARS-CoV-2 Spike RBD. We showed that both S-RBD-Sec and S-RBD-TM grew to high titre and induced the expression of RBD *in vitro* upon infection. We showed that S-RBD-TM, when given intranasally, elicited robust serum antibody response against SARS-CoV-2. We then tested if a heterologous prime-boost regimen with a genetically distant sarbecovirus RBD can improve the breadth of immune response. We produced S-RBD-TM BM48-31 (a Clade 3 sarbecovirus RBD) and showed that a S-RBD-TM Wuhan/S-RBD-TM BM48-31 prime-boost regimen moderately increases antibody breadth against mismatched sarbecoviruses compared to homologous prime-boost with S-RBD-TM Wuhan. Together, our results highlight S-RBD-TM as a promising vaccine candidate for broader protection against sarbecoviruses.

Results

Generation and characterisation of X31 H3 S-RBD

To generate S-FLU capable of expressing the SARS-CoV-2 RBD, the coding region of the haemagglutinin in the HA vRNA was replaced with the sequence encoding the RBD from the SARS-CoV-2 Spike based on the original Wuhan strain (HA-RBD). In addition to the HA-RBD segment, these viruses contain the other seven internal vRNAs gene segments from H1N1 A/Puerto Rico/1/1934 (PR8). Two versions of S-RBD were generated; S-RBD-Sec (expressing soluble RBD) and S-RBD-TM (expressing a membrane-anchored form of the RBD). To generate S-RBD-TM, we fused a signal peptide (from H7 Influenza HA) to the N-terminus of the RBD coding sequence, and added a transmembrane domain (TM) and cytoplasmic domain at the C-terminus (sourced from various proteins). The 3' and 5' packaging sequences of the HA vRNA were retained to facilitate viral packaging (Figure 1A). The S-RBD-Sec contains the same sequence as the S-RBD-TM but lacks the transmembrane domain to allow secretion. Both S-RBD-Sec and S-RBD-TM were generated using reverse genetics in HEK293T cells. These S-RBD viruses lack a functioning HA vRNA, therefore HA was supplied *in trans* in producer MDCK cells to allow viral packaging. For the S-RBD-TM, we first tested the native PR8 H1 haemagglutinin transmembrane and cytoplasmic domain but failed to rescue any virus (data not shown). We hypothesised that the PR8 H1 TM and cytoplasmic domain interfered with virion packaging. We then tested alternative TMs: the mouse CD80 TM as previously

described [47], the influenza N7 neuraminidase TM (a type II glycoprotein), and the SARS-CoV-2 Spike TM (with the last 18 amino acids at the N-terminus deleted to increase surface expression) [50]. All three constructs permitted successful virus rescue, evident by expression of influenza viral protein and SARS-CoV-2 RBD in infected cells (Figure S1). Both SARS-CoV-2 spike and mouse CD80 TM expressed comparable levels of RBD (based on influenza NP and RBD staining in infected cells) whereas most cells infected with the N7 TM demonstrated marginal RBD expression if any. Based on these results, we proceeded with the SARS-CoV-2 Spike TM domain for S-RBD-TM. Rescued S-RBD-TM and S-RBD-Sec seed viruses were then propagated in MDCK-SIAT1 cells stably transfected to express the X31 H3N2 (A/H3N2/Aichi/1/1968) HA on the cell surface (MDCK-X31). The viruses were then harvested, and the infectious titre (CI_{D50}) was determined as previously described [51, 52].

To assess RBD expression, MDCK-SIAT1 cells were infected with multiplicity of infection (MOI) 0.01 of the S-RBD-TM and S-RBD-Sec, S-eGFP (an S-FLU expressing GFP), or remained uninfected. After overnight incubation, the infected cells were stained with EY-6A, a class 4 anti-RBD monoclonal antibody (mAb) known to bind to all sarbecovirus RBDs [33]. The results show that both S-RBD-TM and S-RBD-Sec led to expression of RBD in the infected cells (Figure 1B).

To quantify the proportion of S-RBD infection events that result in detectable RBD expression, MDCK-SIAT1 cells were infected with MOI 0.1 of the S-RBD-TM, S-RBD-Sec, or remained uninfected. Co-staining for influenza NP and RBD in the infected cells was performed and analysed by flow cytometry. Infection frequencies, based on NP staining, were comparable between S-RBD-TM and S-RBD-Sec, with approximately 10-15% NP-positive cells detected under both conditions. In S-RBD-TM-infected cells, approximately 45% of NP-positive cells were RBD-positive, whereas no RBD signal was detected in uninfected controls. Only low RBD signal was detected in S-RBD-Sec-infected cells under the same conditions, consistent with secretion of the expressed RBD (Figure 1C). These data indicate that a substantial fraction of S-RBD-TM infection events leads to detectable surface RBD expression in infected cells.

To further evaluate whether RBD is functionally exposed on S-RBD virions, neutralisation assays were performed using two anti-RBD neutralising mAb (FI-3A and C118) [33, 41]. Both S-RBD-TM and S-RBD-Sec were inhibited by an anti-HA mAb, MEDI8852 [53], confirming HA-dependent infection. No inhibition of S-RBD-TM and S-RBD-Sec infection was observed with the anti-RBD neutralising mAbs (Figure S2), suggesting that RBD is not accessible on the viral particle surface at levels sufficient to mediate antibody-dependent neutralisation under these experimental conditions.

Overall, these results show that both S-RBD-TM and S-RBD-Sec support RBD expression following infection in a subset of infected cells, while functional data do not support appreciable RBD display on virions.

Mice vaccinated with S-RBD generate robust systemic anti-RBD antibody responses

To determine if S-RBD-TM and S-RBD-Sec induce an anti-RBD antibody response *in vivo*, mice (female C57BL/6, 5 weeks old) were immunised twice, two weeks apart, intranasally (IN) or intramuscularly (IM) with 5.5×10^5 CID₅₀ of either S-RBD-TM, S-RBD-Sec, or S-eGFP as a mock control (Figure 2A). Sera were collected 2 weeks post-prime and at 3 weeks post-boost. Serum anti-RBD IgG antibody responses were measured using RBD ELISAs (Figure 2B, C) and authentic virus neutralisation assays (Figure 2D) [54-56]. The data show that the intranasal route induces a generally higher serum anti-RBD binding response than the intramuscular route, and the S-RBD-TM is more immunogenic than the S-RBD-Sec when the same dose is given. In addition, the S-RBD-TM administered intranasally successfully produced neutralising titres against authentic SARS-CoV-2, while the other administrations produced titres below the assay limit of detection. Based on these results, we selected the S-RBD-TM and intranasal route for subsequent immunisations.

Heterologous prime-boost regimen of S-RBD increases breadth of binding antibody response against sarbecoviruses

Mounting evidence suggests that heterologous prime-boost immunisation regimens with antigenically distant antigens can induce broad immunity [57-59]. To investigate the potential of a heterologous prime-boost strategy in improving the breadth against sarbecoviruses, a second modified S-RBD-TM based on the distant Clade 3 bat

sarbecovirus BM48-31 was generated using the approach described above. The titre of the virus (namely S/US/RBD-BM48-31-TM (Spike)/N1 PR8/ H3 X31) was 6.16×10^7 $\text{CID}_{50}/\text{mL}$. We hypothesised that a heterologous S-RBD-TM Wuhan/ S-RBD-TM BM48-31 prime-boost regimen could increase the breadth of antibody responses against mismatched sarbecoviruses across different clades and SARS-CoV-2 VOCs. Mice (female, C57BL/6) were immunised intranasally twice, 3 weeks apart, with either a homologous S-RBD-TM Wuhan prime-boost regimen (homologous), a heterologous S-RBD-TM Wuhan/ S-RBD-TM BM48-31 prime-boost regimen (heterologous) or with a homologous S-eGFP prime-boost regimen as a control (mock) (Figure 3A). Sera and bronchoalveolar lavage (BAL) were collected 3 weeks post-boost, and the antibody response was measured. To assess whether the heterologous prime-boost regimen elicited broad-spectrum antibodies against SARS-CoV-2 variants of concern (VOCs), post-boost sera were assessed by ELISA for binding to a broad panel of SARS-CoV-2 VOC Spike proteins (Figure 3B) and to RBDs from sarbecovirus strains (Figure 3C). The ELISA binding data are presented as line plots with significant differences between the different dosing cohorts determined by pairwise comparisons for each strain tested. Spike ELISA results are interpreted as measures of SARS-CoV-2 variant reactivity, whereas RBD ELISA data reflect cross-sarbecovirus binding breadth; conclusions are therefore drawn within each assay type rather than across Spike and RBD binding results.

Serum antibody binding to SARS-CoV-2 VOCs Spike proteins tested (Wuhan, Beta, BA.2, and BA.2.75) could be detected in both the homologous and heterologous groups, whereas no binding activity was detected in the mock treated group. No significant difference was observed between the homologous and heterologous group in terms of binding titres against all Spikes tested (Figure 3B).

We then assessed whether the heterologous prime-boost regimen could increase the cross-reactivity of serum antibodies against sarbecoviruses compared to homologous prime-boost with S-RBD-TM Wuhan. RBD-binding antibody titres were measured by ELISA against a panel of 8 sarbecovirus RBDs, of which 6 were mismatched or partially matched, with BM48-31 being matched to the heterologous group. The serum binding titre to sarbecovirus RBDs of both the homologous and heterologous group

were significantly higher than the S-eGFP control group ($p < 0.01$ and $p < 0.0001$, respectively). Notably, the heterologous group elicited a significantly higher serum binding titre to sarbecovirus RBDs compared to the homologous group ($p < 0.0001$) (Figure 3C). The difference in serum antibody binding titre between the homologous and heterologous group was most pronounced against BM48-31, which is antigenically matched to the heterologous boost group. The heterologous group also showed increased binding to a few of the RBDs tested, such as Pang17, WIV1, and Rf1, compared to the homologous group.

We next evaluated the neutralisation potency of serum antibodies with authentic neutralisation assays against representative SARS-CoV-2 Wuhan, Beta, BA.5 and XBB.1.5 variants, and pseudovirus neutralisation assays. Neutralisation analyses were restricted to viruses for which validated systems were available, and therefore conclusions regarding functional neutralisation breadth are limited to this defined panel. No differences were seen between the homologous and heterologous groups, with both groups eliciting significantly higher neutralisation titres against SARS-CoV-2 Wuhan compared to the S-eGFP group (ID_{50} : homologous: 1:1,216 and heterologous: 1:1,499, $p < 0.01$) (Figure 3D). The homologous group elicited significantly higher serum neutralising titre against the Beta strain ($p < 0.001$) but there was no significant difference for neutralisation against the Beta strain between the homologous and heterologous group (ID_{50} : homologous: 1:283, and heterologous: 1:118). No mice in the homologous group showed neutralisation against BA.5. However, 1 of the 6 mice in the heterologous group had detectable neutralising activity (ID_{50} : 1:956). Neither group showed neutralisation activity against XBB.1.5.

To assess the neutralisation potency against sarbecoviruses, *in vitro* neutralisation assays were performed using pseudoviruses (SARS-CoV-2 Wuhan, WIV1, SARS1, and BtKY72), as previously described [60] (Figure 3E). Both homologous and heterologous groups elicited significantly higher neutralisation titres against the SARS-CoV-2 Wuhan pseudovirus, compared to the S-eGFP mock control group (ID_{50} : 1:2,704 and 1:5,376, $p < 0.05$ and $p < 0.01$, respectively). For the shared Wuhan strain, the pseudovirus neutralisation results were consistent with those obtained using authentic virus (Figure 3D), supporting the reliability and internal concordance of the

assay systems. In addition, correlation analysis between pseudovirus and authentic virus neutralisation titres demonstrated strong agreement (R^2 0.9443, $p < 0.0001$, Figure S3), further supporting assay concordance.

In contrast, cross-neutralisation against other sarbecoviruses was limited (Figure 3E). For WIV1, no neutralising activity was detected in the homologous group, while only 2 of the 6 mice in the heterologous group showed detectable neutralising activity (ID_{50} : 1:644 and 1:132, respectively). Similarly, against BtKY72, all mice in the homologous group failed to elicit neutralising activity, and only one mouse in the heterologous group exhibited neutralising activity (ID_{50} : 1:565). For SARS-1, a single mouse in the homologous group showed neutralisation activity (ID_{50} : 1:143), whereas no mice in the heterologous group showed detectable neutralisation activity. The results indicate that the increased binding breadth observed by ELISA does not uniformly translate into functional cross-neutralising activity within the tested virus panel. Alternative antigen design strategies, such as mosaic or multi-epitope RBD constructs may represent potential avenues to improve functional neutralisation breadth.

To assess local antibody responses in the airways, the IgA response against Wuhan RBD in BAL was measured. Both the homologous and heterologous groups elicited significantly higher RBD IgA responses compared to the control S-eGFP group ($p < 0.05$) (Figure 3F). The difference in IgA responses between the homologous and heterologous group was not statistically significant.

Discussion

The emergence of SARS-CoV-2 variants and the ongoing threat of zoonotic sarbecovirus underscores the need for pan-sarbecovirus vaccines. Such vaccines could offer a proactive defence against future epidemics and pandemics. Broadly reactive vaccines may eliminate the need for strain-specific formulations, which would mark a ground-breaking shift in pandemic preparedness. The identification of numerous cross-neutralising antibodies, specifically targeting conserved RBD class 3, 4, 1/4 and 5 epitopes [33, 34, 36-39, 41-43], support the feasibility of sarbecovirus RBDs as a promising target for broadly reactive vaccine strategies.

In this study, we generated and characterised two versions of S-FLU expressing the SARS-CoV-2 RBD: a soluble form (S-RBD-Sec) and a membrane-anchored form (S-RBD-TM). The use of S-FLU as a candidate vaccine offers several compelling advantages. Notably, S-FLU exhibits the capacity to infect host cells but is replication-incompetent; this controlled infection facilitates small droplet aerosol administration directly to the respiratory tract to elicit mucosal immunity [45, 61, 62]. Both S-RBD constructs were efficiently rescued using reverse genetics and demonstrated robust RBD expression in infected cells. However, our findings also indicate that RBD expression following S-RBD-TM infection is heterogenous at the single-cell level, with approximately half of the infected cells (NP-positive) showing detectable RBD expression. This partial penetrance may reflect variability in transcriptional activity of the RBD transgene, difference in the timing of viral gene expression relative to detection, and potentially emergence of mutations affecting RBD transgene expression during rescue or early replication cycles. The lack of detectable RBD signal in S-RBD-Sec-infected cells under the same conditions is consistent with efficient secretion and/or reduced intracellular retention of RBD. Despite the heterogeneity, immunisation studies in mice revealed that both S-RBD constructs elicited systemic anti-RBD antibody responses, with S-RBD-TM showing superior immunogenicity, particularly via the intranasal route. These results indicate that even transient or subset expression of the RBD is sufficient to drive antigen presentation and adaptive immune responses. Although T-cell responses were not evaluated in this study, we previously shown that S-FLU can elicit both local lung and systemic CD8 T-cell responses to the transgene it carries, which could further enhance the overall immunogenicity of S-RBD [45, 63]. In addition, our neutralisation data provide insight into whether the RBD is displayed on the surface of S-RBD virions. Anti-RBD neutralising monoclonal antibodies failed to inhibit infection in cell culture, indicating that RBD is not functionally exposed on the virion surface at levels sufficient to mediate antibody-dependent neutralisation. This finding supports a model in which the RBD antigen is predominantly expressed following entry in infected host cells rather than being incorporated into or displayed on viral particles at appreciable density. Importantly, infection remained fully susceptible to inhibition by the anti-HA monoclonal antibody MEDI8852, confirming that viral entry is HA-dependent. While we cannot exclude the possibility of low-level or stochastic incorporation of RBD into virions, such events are unlikely to contribute meaningfully to the overall

immunogenicity of the vaccine platform. Together, these results suggest a mechanism in which immune priming is driven primarily by intracellular antigen expression, rather than by direct antigen display on virions.

To enhance the breadth of the antibody response, we employed a heterologous prime-boost strategy using antigenically distinct RBDs derived from the SARS-CoV-2 Wuhan strain and the Clade 3 bat sarbecovirus BM48-31. This approach broadened the binding antibody responses against sarbecoviruses, although no significant differences in neutralisation potencies were observed between homologous and heterologous regimens. This suggests that binding does not always correlate with functional neutralisation, and further optimisation may be needed to enhance cross-neutralising activity. Nevertheless, these non-neutralising antibodies could have a protective role, via Fc-mediated effector functions, as have been previously shown to aid in prevention of severe COVID-19, although this was not directly evaluated in the present study [64-66]. Consequently, our findings do not provide explicit evidence to suggest that the heterologous prime-boost regimen has any discernible effect on breadth against mismatched SARS-CoV-2 VOCs. This is conceivable as VOCs are still closely related to the Wuhan strain (Table S1), and a heterologous boost with a distantly related virus may not enhance the breadth of responses.

A key advantage of the S-FLU system is its capacity to be pseudotyped avian influenza haemagglutinin subtypes (such as H5 or H7), against which there is little to no pre-existing immunity in the populations, thereby potentially reducing interference from prior influenza exposure. We have previously demonstrated that alternating HA pseudotypes can circumvent vector immunity in mice [63], suggesting a feasible strategy to mitigate anti-vector effects upon repeated dosing. A potential limitation of S-FLU and influenza-based RNA vector systems more broadly, is the intrinsic error-prone nature of the viral RNA-dependent RNA polymerase, which could potentially affect the genetic stability of inserted transgenes during viral rescue or amplification. This could contribute, in part, to the observed heterogeneity in RBD expression in S-RBD-TM infected cells. Accordingly, the stability of the RBD insert during manufacturing and scale-up remains an important consideration for translational development. Genetic integrity of the transgene would need to be carefully monitored during production to ensure consistency and product stability.

There are several limitations in this study. First, we did not directly assess the protective efficacy of S-RBD-TM against SARS-CoV-2 in a viral challenge model. Such studies could help define potential protective effects of non-neutralising antibodies. Second, tissue resident CD4⁺ and CD8⁺ T cell activity in the airways was not evaluated, which has been shown to correlate with protection and reduced disease severity against SARS-CoV-2 infection in mice [67, 68]. Next, although we showed robust antibody responses at 3-week post boost, the longevity of the antibody response was not determined. In addition, we did not directly evaluate tissue tropism or *in vivo* RBD expression following intranasal and intramuscular immunisation. Previous studies have demonstrated that S-FLU can infect murine respiratory tracts and express its encoded transgene following intranasal administration [52]. Future studies examining *in vivo* antigen expression, tissue tropism, and cellular immune responses will further clarify the mechanisms underlying the immunogenicity of this platform.

In summary, our findings demonstrate the potential of S-FLU-based RBD intranasal vaccines to elicit both local and systemic antibody responses and provide a framework for future optimisation of a pan-sarbecovirus vaccine design.

Material and Methods

Plasmids

Plasmids used for reverse genetics for S-RBD-TM production are; 6 pPol plasmids encoding the vRNA (pPol_PB1-PR8, pPol_PB2-PR8, pPol_PA-PR8, pPol_NP-PR8, pPol_NS-PR8, pPol_M-PR8, pPol_N1-PR8), 4 core initiators to supply essential viral proteins *in trans* for vRNA replication and viral packaging (pCDNA3.1_PB1-PR8, pCDNA3.1_PB2-PR8, pCDNA3.1_PA-PR8, pCDNA3.1_NP-PR8), pCDNA3.1_H1_HA-PR8 (to supply HA *in trans* on the producer cells' surface) and either pPol/US/RBD (Wuhan)-TM, pPol/US/RBD (BM48-31)-TM or pPol/US/eGFP. pPol/US/eGFP had previously been synthesised for proof of principle experiments [45]. The cDNA fragment (mammalian signal sequence-BM48-31 RBD- SARS-CoV-2 Spike Transmembrane Domain flanked by *NotI* and *EcoRI* sites) was designed and synthesised by Twist Bioscience. 3,000ng of the cDNA fragment from Twist

Bioscience was digested with *NotI* and *EcoRI* at 37°C for 30 min in a 40µL reaction containing 4µL of CutSmart buffer and 20 units of *NotI* and *EcoRI*, respectively. Digested cDNA fragment was purified using a QIAquick PCR purification kit. The digested cDNA fragment was then eluted in 25µL of nuclease free water, of which 6µL was incubated with 2µL of vector (PV-pPol_HA *EcoRI-NotI*) (previously prepared in the laboratory), 1µL T4 DNA ligase buffer and 1µL T4 DNA ligase at 25°C for 30 min. 5µL of the ligation reaction was then used to transform 10µL of *E.coli* DH5-alpha competent cells that were plated on an Ampicillin LB agar plate. The agar plate was incubated at 37°C overnight. 4 colonies were then picked and grown in LB broth overnight in a shaking incubator (200 rpm). Plasmid DNA was then extracted by alkaline lysis method using a ZymoPURE Plasmid Miniprep kit. The sequence of the extracted plasmid minipreps was confirmed using Sanger sequencing.

Cell lines

The MDCK-SIAT1 cell line used in this study was obtained from the European Collection of Authenticated Cell Cultures (ECACC) (catalogue number 05071502). MDCK-X31 cells were generated in house by stable lentiviral transfection of MDCK-SIAT1 to express the full-length haemagglutinin from influenza A/H3N2 (A/Aichi/1/1968) (X31). HEK293T cells (ECACC catalogue number 12022001) used in this study were a kind gift from Ervin Fodor (Sir William Dunn School of Pathology, University of Oxford). The 293T_{ACE2} used for pseudovirus neutralisation assays was obtained from BEI resources (catalogue number NR-52511). Vero CCL81 used in authentic virus neutralisation assays was obtained from ATCC (catalogue number CCL-81). The Expi293F cell line used for the production of recombinant Spike and RBD proteins was obtained commercially from Thermo Fisher Scientific (catalogue number A14527)

Generation of S-FLU viruses

S-FLU (S-RBD) viruses were generated by reverse genetics, as described [45] with slight modifications. Briefly, 1e6 of HEK293T cells were seeded in a 6 well-plate in 2 mL D10 (Dulbecco's modified Eagle's medium (DMEM) with 10% heat inactivated foetal bovine serum, 2 mM L-glutamine, 1% penicillin and streptomycin). 24 h later, media was exchanged to serum-free OptiMEM media and 1µg of each plasmid was

used to transfect the HEK293T cells using the Lipofectamine2000 (ThermoFisher) transfection reagent. 4 h post-transfection, media was replaced with 2 mL of viral growth media (VGM; DMEM, 1% penicillin & streptomycin, 2mM L-glutamine, 0.1% BSA, 10mM HEPES) containing 1 $\mu\text{g}/\text{mL}$ TPCK-treated trypsin.

Approximately 72h post-transfection, the supernatant containing seed virus was harvested and clarified via centrifugation at 1400 x g for 5 min. MDCK-X31 cells ($1\text{e}6/\text{well}$) seeded in 6-well plate the day before were infected with the seed virus for 1 h at 37 °C. Media was then replaced with 2 mL VGM containing 1 $\mu\text{g}/\text{mL}$ TPCK-treated trypsin 1 h post-infection and plates were incubated at 37 °C. The propagated virus (S-RBD-TM) was harvested 48h post-infection. The S-RBD-TM was further propagated by infecting the 2 mL (diluted in 10 mL of VGM) of virus in a T175 seeded with $5\text{e}6$ MDCK-X31 the day before. After 1 h of incubation at 37 °C, media was replaced with 40mL of fresh VGM containing 1 $\mu\text{g}/\text{mL}$ of TPCK-treated trypsin. After 48 h, supernatant containing the virus was harvested and clarified via centrifugation at 1400 x g for 5 min to pellet any cellular debris. Harvested virus was aliquoted and stored at -80 °C.

Virus titration (CID_{50})

Viral titres were determined by fifty percent cell culture infectivity dose (CID_{50}) in MDCK-SIAT1 indicator cells as previously described with slight modifications. Briefly, MDCK-SIAT1 cells ($3\text{x}10^4/\text{well}$) seeded in a flat-bottomed 96-well plate were infected with harvested virus in a 2-fold dilution series. After overnight incubation at 37°C, the media was removed, and 100 μL of 10% formalin in PBS was added at 4 °C for 30 min. The plates were washed twice with PBS and stained with 50 μL of 10 $\mu\text{g}/\text{mL}$ of EY-6A (anti-RBD human IgG1 monoclonal antibody (binds to all SARS-like betacoronavirus RBD)[69] in PBS/0.1% BSA and incubated for 1 h at RT on a plate shaker. For S/US/RBD-Sec/N1 PR8/H3 X31, infected cells were permeabilised for 20 min at RT with PBS/ 0.5% Triton-X/ 20mM glycine prior to staining. The primary antibody was then removed, and the wells were washed twice with PBS and incubated for 1 h on a plate shaker with 50 μL of Goat-Anti-Human (GAH) AF647 (1:500) in PBS/0.1% BSA. After washing with PBS, 100 μL of 1% formalin (0.4% paraformaldehyde) was added to each well, and plates were read using a Clariostar

spectrophotometer (BMG Labtech). The $\text{CID}_{50}/\text{mL}$ was calculated as previously described [51, 52], and the titres are: S/US/RBD-Sec/N1 PR8/H3 X31: 7.68×10^7 $\text{CID}_{50}/\text{mL}$, S/US/RBD-TM/N1 PR8/H3 X31: 1×10^7 $\text{CID}_{50}/\text{mL}$, S/US/RBD-BM48-31-TM (Spike)/N1 PR8/ H3 X31: 6.16×10^7 $\text{CID}_{50}/\text{mL}$.

RBD expression confirmation *in vitro*

MDCK-SIAT1 cells (1×10^6 /well) were cultured overnight in 6-well plates with 2 mL of D10 at 37 °C. Media was then replaced with 0.5×10^6 CID_{50} of virus in 1 mL of VGM and incubated overnight at 37 °C. After removal of the media, 1 mL of 10% formalin was added and incubated at 4 °C for 30 min. The plate was washed twice with 1 mL PBS, then EY-6A IgG (10 $\mu\text{g}/\text{mL}$ in 1 mL PBS/0.1% BSA) was applied and incubated at RT for 1 h. After washing, Goat Anti-Human-AF647 (1:500 in 1 mL PBS/0.1% BSA) was added, and the plate was incubated for 1 h at RT. Following two washes with 1 mL PBS, 1 mL of 1% formalin was added per well for fluorescence microscopy. To quantify the proportion of RBD-positive cells among S-RBD-infected cells, 1×10^6 MDCK-SIAT1 cells were infected with MOI 0.1 of S-RBD-TM, or S-RBD-Sec, or left uninfected as controls. Cells were incubated at 37 °C overnight. For S-RBD-TM-infected cells and uninfected controls, cells were washed twice with PBS and stained with an anti-RBD monoclonal antibody (EY-6A) conjugated to AF488 for 30 min at room temperature. Cells were then fixed with 10% formalin and permeabilised prior to staining with an anti-NP monoclonal antibody (2-8C) [45] conjugated to AF647 for 30 min. For S-RBD-Sec-infected cells, samples were washed twice with PBS, fixed with 10% formalin, and permeabilised prior to simultaneous staining with EY-6A-AF488 and 2-8C-AF647 for 30 min. All samples were stained with Zombie Violet viability dye according to the manufacturer's instructions. Cells were analysed by flow cytometry using an Attune NxT instrument (Thermo Fisher Scientific), and data were processed in FloJo (BD Biosciences) to quantify the proportion of NP-positive cells expressing RBD.

Microneutralisation Assays

Microneutralisation assays were performed as previously described [45]. Briefly, serial (2-fold) dilutions of mAb were incubated with S-RBD diluted in Viral Growth Media (VGM; DMEM-penicillin-streptomycin-0.1% BSA) for 2 h at 37 °C. A total of 3×10^4

MDCK-ACE2 (MDCK-SIAT1 cells stably expressing human ACE2) cells were then added in 100 μ L of VGM and incubated overnight at 37°C. Cells were subsequently fixed with 10% formalin for 30 min at 4 °C, followed by permeabilisation for 20 min at room temperature. Infection was quantified by staining with a biotinylated anti-nucleoprotein (NP) monoclonal antibody (2-8C), followed by streptavidin-Alexa Fluor 647 secondary detection. Fluorescence intensity was measured using a Clariostar Spectrophotometer (BMG Labtech).

Mice and immunisation

Mice used in this study were purchased from Envigo Ltd., UK and procedures carried out at the Biomedical Services Unit (BMS) (University of Oxford, United Kingdom) in accordance with the UK Animals (Scientific Procedures) Act 1986 and with approval from the local Animal Welfare and Ethical Review Body (AWERB) (Project Licence PP9362617), and are reported in accordance with the ARRIVE guidelines. Mice were housed in accordance with the UK Home Office ethical and welfare guidelines and fed on standard chow and water *ad libitum*. Female C57BL/6 mice at 4-6 weeks of age were used in this study. For intranasal delivery, mice were lightly anaesthetised with inhaled isoflurane and 50 μ L of S-RBD was delivered via the nostrils. For intramuscular delivery, mice were anaesthetised with inhaled isoflurane and 50 μ L of S-RBD was injected using an insulin needle into the thigh muscle. Post prime blood was collected via the tail vein using a capillary tube. Mice were euthanized by gradual chamber fill with compressed CO₂ (displacement rate: 30–70% of chamber volume per minute). Sera were collected by cardiac puncture, with whole blood drawn into Microtainer SST tubes (BD). Samples were clotted at room temperature for 1 h, centrifuged at 10,000 \times g for 5 min, and the clarified sera were heat-inactivated at 56 °C for 30 min before storage at –20 °C. To collect BAL, the trachea of euthanised mice was exposed by blunt dissection, and a small incision was made to insert a cannula (0.75 mm, Harvard Apparatus, UK) attached to a 21G needle. The cannula was advanced until positioned just above the carina. A 1 mL syringe was used to instil PBS into the lungs, followed by gentle aspiration to recover the fluid. This procedure was repeated twice, and the collected lavage was stored at –20 °C until further processing.

Production of soluble Spike and RBD for ELISA

The SARS-CoV-2 and VOCs Spikes (HexaPro) (Wuhan, Beta, BA.2 and BA.2.75) were previously produced in the laboratory using the method described below. The plasmids encoding soluble sarbecovirus RBD (RBD-6H or RBD-ST1 (Wuhan), BM48-31-AviTag, Pang17-AviTag, WIV1-AviTag, Rs4081-AviTag, RmYN02-AviTag, Rf1-AviTag) were expressed in Expi293 cells via transient transfection according to the manufacturer's instructions. At day 6-7 post-transfection, expressed proteins were purified from culture supernatants via immobilised nickel affinity chromatography (IMAC) using an automated protocol implemented on an AKTASart system (GE Healthcare). Affinity-purified proteins were diafiltered and concentrated into PBS using 10k MWCO Amicon spin filters. Protein concentrations were determined from A_{280} measurements using a Nanodrop Spectrophotometer (ThermoFisher).

Serum IgG ELISA

ELISAs were conducted as previously described [54]. Briefly, 50 μL of 2 $\mu\text{g}/\text{mL}$ of purified RBD or 1 $\mu\text{g}/\text{mL}$ of trimeric Spike (HexaPro)[70] proteins diluted in PBS were added to each well of Maxisorp NUNC plates (Thermo Fisher Scientific) overnight at 4 °C or at RT for 1-2h on a plate shaker. Plates were washed 3 times with PBS and blocked with 300 μL of 5% skim milk in PBS for 1 h at RT on a plate shaker or overnight at 4 °C. In round bottomed 96-well plates, mouse sera were diluted (starting dilution 1:100) in PBS/0.1% BSA in a half-log serial dilution in duplicate. NUNC plates were washed with PBS and 50 μL of the diluted sera was transferred to the coated NUNC plates for 1 h at RT before being washed with PBS 3 times. The secondary HRP conjugated goat anti-mouse immunoglobulin antibody (Dako P0447) was diluted 1:800 in PBS/0.1% BSA, and 50 μL were added into each well of the NUNC plate for 1 h at RT. Plates were then washed and developed with 50 μL of KPL SureBlue substrate for 5 min and stopped with 50 μL of 1M H_2SO_4 . Absorbance (OD_{450}) was measured on a Clariostar spectrophotometer (BMG Labtech). ELISA titres were calculated and presented as Area Under Curve (AUC).

Authentic virus microneutralisation assays (SARS-CoV-2 VOCs)

Microneutralisation assays against authentic SARS-CoV-2 viruses were conducted as described [55, 56]. Triplicate serial dilutions of sera (20 μ L) were pre-incubated with 100 focus-forming units (FFUs) of virus for 30 min at RT. After pre-incubation, 100 μ L Vero CCL81 cells (4.5×10^4) were added and incubated at 37 °C, 5% CO₂. 2h later, 100 μ L of a 1.5% carboxymethyl cellulose-containing overlay was added to prevent satellite focus formation. 20 h (Wuhan), 18 h (Beta) and 22 h (Omicron BA.5 and XBB.1.5) post-infection, monolayers were fixed with 4% paraformaldehyde at RT for 30 min, permeabilised with 100 μ L 2% Triton X-100 for 30 min at 37°C and stained for the nucleoprotein with FB-9B. After development with a peroxidase-conjugated antibody and TrueBlue peroxidase substrate, infectious foci were enumerated by ELISpot reader. Half-maximal inhibitory dilutions (ID₅₀) were assessed using 4-parameter nonlinear regression in GraphPad Prism 10. Assays were performed in a containment level three facility under a license from the Health and Safety Authority, UK.

Pseudovirus neutralisation assays (sarbecoviruses)

Pseudoviruses based on a lentiviral vector were prepared as described [35, 71] using genes encoding S protein sequences lacking C-terminal residues in the cytoplasmic tail: 21 residue (SARS-CoV-2 Wuhan and WIV1) or 19 residue cytoplasmic tail deletions (SARS-CoV, BtKY72/SARS-1 chimera). For neutralisation assays, pseudovirus was incubated with three-fold serially diluted sera from immunised mice for 1 h at 37 °C, then the serum/virus mixture was added to 293T_{ACE2} target cells. After 48h incubation, media was removed, and cells were lysed with Britelite Plus reagent (Perkin Elmer), and luciferase activity was measured as relative luminescence units (RLUs). Relative RLUs were normalised to RLUs from cells infected with pseudovirus in the absence of serum. Half-maximal inhibitory dilutions (ID₅₀) were derived using 4-parameter nonlinear regression in AntibodyDatabase [72].

Statistical Analysis

Pairwise comparisons were performed (Figure 3B and 3C), as described previously [73], to evaluate sets of binding titre against individual RBD across different immunisation cohorts and to determine whether results between cohorts were significantly different. Statistical differences in ELISA and neutralisation titres between

immunised groups were assessed using analysis of variance (Kruskal-Wallis), followed by Dunn's correction test, pairing by Spike/RBD protein or viral strain. Statistical analysis was performed using GraphPad Prism version 10. Statistical significance is represented as * $p < 0.05$, ** $p < 0.01$, *** $p < 0.001$, **** $p < 0.0001$.

Author Contributions

Conceptualisation: T.K.T, A.R.T. Methodology: J.M., T.K.T. Investigation: J.M., T.K.T., D.M., L.S., M.A., A.C., J.R.K. Supervision: A.R.T., T.K.T. Writing (original draft): J.M., T.K.T. Writing (review and editing): T.K.T, W.S.J., J.R.K, P.J.B., A.R.T.

Funding

The work was funded by the Townsend-Jeantet Charitable Trust (charity number 1011770), the COVID Response Fund (University of Oxford), and the National Institutes of Health (P01-AI165075 to P.J.B.).

Acknowledgments

We would like to express our gratitude to the staff members at the Biomedical Science Services, John Radcliffe Hospital (Oxford University) for their assistance with the mouse experiments. This manuscript is the result of funding in whole or in part by the National Institutes of Health (NIH). It is subject to the NIH Public Access Policy. Through acceptance of this federal funding, NIH has been given a right to make this manuscript publicly available in PubMed Central upon the Official Date of Publication, as defined by NIH.

Competing interests

The authors declare that they have no competing interests.

Data Availability

All data supporting the findings of this study are provided within the manuscript and its Supporting Information files. All reagents generated in this study, including plasmids and protein constructs, are available from the corresponding author upon reasonable request, subject to institutional Material Transfer Agreement.

Reference

1. Wu, F., et al., *Author Correction: A new coronavirus associated with human respiratory disease in China*. *Nature*, 2020. **580**(7803): p. E7.
2. Zhou, P., et al., *Addendum: A pneumonia outbreak associated with a new coronavirus of probable bat origin*. *Nature*, 2020. **588**(7836): p. E6.
3. Sachs, J.D., et al., *The Lancet Commission on lessons for the future from the COVID-19 pandemic*. *Lancet*, 2022. **400**(10359): p. 1224-1280.
4. Carreno, J.M., et al., *Activity of convalescent and vaccine serum against SARS-CoV-2 Omicron*. *Nature*, 2022. **602**(7898): p. 682-688.
5. Deng, X., et al., *Transmission, infectivity, and neutralization of a spike L452R SARS-CoV-2 variant*. *Cell*, 2021. **184**(13): p. 3426-3437 e8.
6. Liu, C., et al., *Reduced neutralization of SARS-CoV-2 B.1.617 by vaccine and convalescent serum*. *Cell*, 2021. **184**(16): p. 4220-4236 e13.
7. Tegally, H., et al., *Detection of a SARS-CoV-2 variant of concern in South Africa*. *Nature*, 2021. **592**(7854): p. 438-443.
8. Volz, E., et al., *Assessing transmissibility of SARS-CoV-2 lineage B.1.1.7 in England*. *Nature*, 2021. **593**(7858): p. 266-269.
9. Collier, D.A., et al., *Author Correction: Sensitivity of SARS-CoV-2 B.1.1.7 to mRNA vaccine-elicited antibodies*. *Nature*, 2022. **608**(7922): p. E24.
10. Takashita, E., et al., *Efficacy of Antibodies and Antiviral Drugs against Omicron BA.2.12.1, BA.4, and BA.5 Subvariants*. *N Engl J Med*, 2022. **387**(5): p. 468-470.
11. Wang, P., et al., *Antibody resistance of SARS-CoV-2 variants B.1.351 and B.1.1.7*. *Nature*, 2021. **593**(7857): p. 130-135.
12. Wibmer, C.K., et al., *SARS-CoV-2 501Y.V2 escapes neutralization by South African COVID-19 donor plasma*. *Nat Med*, 2021. **27**(4): p. 622-625.
13. Cui, J., F. Li, and Z.L. Shi, *Origin and evolution of pathogenic coronaviruses*. *Nat Rev Microbiol*, 2019. **17**(3): p. 181-192.
14. Fung, T.S. and D.X. Liu, *Human Coronavirus: Host-Pathogen Interaction*. *Annu Rev Microbiol*, 2019. **73**: p. 529-557.
15. Li, W., et al., *Bats are natural reservoirs of SARS-like coronaviruses*. *Science*, 2005. **310**(5748): p. 676-9.
16. Sabir, J.S., et al., *Co-circulation of three camel coronavirus species and recombination of MERS-CoVs in Saudi Arabia*. *Science*, 2016. **351**(6268): p. 81-4.
17. Zhong, N.S., et al., *Epidemiology and cause of severe acute respiratory syndrome (SARS) in Guangdong, People's Republic of China, in February, 2003*. *Lancet*, 2003. **362**(9393): p. 1353-8.
18. Drosten, C., et al., *Identification of a novel coronavirus in patients with severe acute respiratory syndrome*. *N Engl J Med*, 2003. **348**(20): p. 1967-76.
19. Nicholls, J.M., et al., *Lung pathology of fatal severe acute respiratory syndrome*. *Lancet*, 2003. **361**(9371): p. 1773-8.
20. Zaki, A.M., et al., *Isolation of a novel coronavirus from a man with pneumonia in Saudi Arabia*. *N Engl J Med*, 2012. **367**(19): p. 1814-20.
21. Elhazmi, A., et al., *Severe acute respiratory syndrome coronavirus 2 (SARS-CoV-2) and Middle East Respiratory Syndrome Coronavirus (MERS-CoV) coinfection: A unique case series*. *Travel Med Infect Dis*, 2021. **41**: p. 102026.

22. van Boheemen, S., et al., *Genomic characterization of a newly discovered coronavirus associated with acute respiratory distress syndrome in humans*. *mBio*, 2012. **3**(6).
23. Ge, X.Y., et al., *Isolation and characterization of a bat SARS-like coronavirus that uses the ACE2 receptor*. *Nature*, 2013. **503**(7477): p. 535-+.
24. Anthony, S.J., et al., *Further Evidence for Bats as the Evolutionary Source of Middle East Respiratory Syndrome Coronavirus*. *Mbio*, 2017. **8**(2).
25. Letko, M., A. Marzi, and V. Munster, *Functional assessment of cell entry and receptor usage for SARS-CoV-2 and other lineage B betacoronaviruses*. *Nature Microbiology*, 2020. **5**(4): p. 562-+.
26. Menachery, V.D., et al., *SARS-like WIV1-CoV poised for human emergence*. *Proceedings of the National Academy of Sciences of the United States of America*, 2016. **113**(11): p. 3048-3053.
27. Wang, N., et al., *Serological Evidence of Bat SARS-Related Coronavirus Infection in Humans, China*. *Virology*, 2018. **33**(1): p. 104-107.
28. Moore, K.A., et al., *A research and development (R&D) roadmap for broadly protective coronavirus vaccines: A pandemic preparedness strategy*. *Vaccine*, 2023. **41**(13): p. 2101-2112.
29. Zhao, F., et al., *Challenges and developments in universal vaccine design against SARS-CoV-2 variants*. *NPJ Vaccines*, 2022. **7**(1): p. 167.
30. Walls, A.C., et al., *Structure, Function, and Antigenicity of the SARS-CoV-2 Spike Glycoprotein*. *Cell*, 2020. **183**(6): p. 1735.
31. Tortorici, M.A. and D. Veasler, *Structural insights into coronavirus entry*. *Complementary Strategies to Understand Virus Structure and Function*, 2019. **105**: p. 93-116.
32. Brouwer, P.J.M., et al., *Potent neutralizing antibodies from COVID-19 patients define multiple targets of vulnerability*. *Science*, 2020. **369**(6504): p. 643-650.
33. Huang, K.A., et al., *Correction: Breadth and function of antibody response to acute SARS-CoV-2 infection in humans*. *PLoS Pathog*, 2021. **17**(12): p. e1010148.
34. Liu, L., et al., *Potent neutralizing antibodies against multiple epitopes on SARS-CoV-2 spike*. *Nature*, 2020. **584**(7821): p. 450-456.
35. Robbiani, D.F., et al., *Convergent antibody responses to SARS-CoV-2 in convalescent individuals*. *Nature*, 2020. **584**(7821): p. 437-442.
36. Barnes, C.O., et al., *SARS-CoV-2 neutralizing antibody structures inform therapeutic strategies*. *Nature*, 2020. **588**(7839): p. 682-687.
37. Huang, K.A., et al., *Structural basis for a conserved neutralization epitope on the receptor-binding domain of SARS-CoV-2*. *Nat Commun*, 2023. **14**(1): p. 311.
38. Pinto, D., et al., *Cross-neutralization of SARS-CoV-2 by a human monoclonal SARS-CoV antibody*. *Nature*, 2020. **583**(7815): p. 290-295.
39. Tortorici, M.A., et al., *Broad sarbecovirus neutralization by a human monoclonal antibody*. *Nature*, 2021. **597**(7874): p. 103-108.
40. Wec, A.Z., et al., *Broad neutralization of SARS-related viruses by human monoclonal antibodies*. *Science*, 2020. **369**(6504): p. 731-736.
41. Jette, C.A., et al., *Broad cross-reactivity across sarbecoviruses exhibited by a subset of COVID-19 donor-derived neutralizing antibodies*. *Cell Rep*, 2021. **37**(12): p. 110188.

42. Jensen, J.L., et al., *Targeting the Spike Receptor Binding Domain Class V Cryptic Epitope by an Antibody with Pan-Sarbecovirus Activity*. J Virol, 2023. **97**(7): p. e0159622.
43. Cui, L., et al., *A cryptic site in class 5 epitope of SARS-CoV-2 RBD maintains highly conservation across natural isolates*. iScience, 2024. **27**(7): p. 110208.
44. Powell, T.J., et al., *A single cycle influenza virus coated in H7 haemagglutinin generates neutralizing antibody responses to haemagglutinin and neuraminidase glycoproteins and protection from heterotypic challenge*. Journal of General Virology, 2019. **100**(3): p. 431-445.
45. Powell, T.J., et al., *Pseudotyped Influenza A Virus as a Vaccine for the Induction of Heterotypic Immunity*. Journal of Virology, 2012. **86**(24): p. 13397-13406.
46. Deng, S., et al., *An intranasal influenza virus-vectored vaccine prevents SARS-CoV-2 replication in respiratory tissues of mice and hamsters*. Nat Commun, 2023. **14**(1): p. 2081.
47. Loes, A.N., et al., *Attenuated Influenza Virions Expressing the SARS-CoV-2 Receptor-Binding Domain Induce Neutralizing Antibodies in Mice*. Viruses, 2020. **12**(9).
48. Moser, M.J., et al., *Intranasal Single-Replication Influenza Vector Induces Cross-Reactive Serum and Mucosal Antibodies against SARS-CoV-2 Variants*. Vaccines (Basel), 2023. **11**(6).
49. Zhao, Y., et al., *An influenza virus vector candidate vaccine stably expressing SARS-CoV-2 receptor-binding domain produces high and long-lasting neutralizing antibodies in mice*. Vet Microbiol, 2022. **271**: p. 109491.
50. Ou, X., et al., *Characterization of spike glycoprotein of SARS-CoV-2 on virus entry and its immune cross-reactivity with SARS-CoV*. Nat Commun, 2020. **11**(1): p. 1620.
51. Xiao, J.H., et al., *Characterization of Influenza Virus Pseudotyped with Ebolavirus Glycoprotein*. J Virol, 2018. **92**(4).
52. Tan, T.K., et al., *Single-cycle, pseudotyped reporter influenza virus to facilitate evaluation of treatment strategies for avian influenza, Ebola and other highly infectious diseases in vivo*. Front Immunol, 2025. **16**: p. 1608074.
53. Kallewaard, N.L., et al., *Structure and Function Analysis of an Antibody Recognizing All Influenza A Subtypes*. Cell, 2016. **166**(3): p. 596-608.
54. Tan, T.K., et al., *A COVID-19 vaccine candidate using SpyCatcher multimerization of the SARS-CoV-2 spike protein receptor-binding domain induces potent neutralising antibody responses*. Nat Commun, 2021. **12**(1): p. 542.
55. Gelinas, A.D., et al., *Broadly neutralizing aptamers to SARS-CoV-2: A diverse panel of modified DNA antiviral agents*. Mol Ther Nucleic Acids, 2023. **31**: p. 370-382.
56. Afzal, M., et al., *Determination of resilience of a panel of broadly neutralizing mAbs to emerging variants of SARS-CoV-2 generated using reverse genetics*. iScience, 2025. **28**(6): p. 112451.
57. Van Reeth, K., et al., *Heterologous prime-boost vaccination with H3N2 influenza viruses of swine favors cross-clade antibody responses and protection*. NPJ Vaccines, 2017. **2**.
58. Bhatnagar, N., et al., *Heterologous Prime-Boost Vaccination with Inactivated Influenza Viruses Induces More Effective Cross-Protection than Homologous Repeat Vaccination*. Vaccines (Basel), 2023. **11**(7).

59. Li, X., et al., *Heterologous prime-boost immunisation with mRNA- and AdC68-based 2019-nCoV variant vaccines induces broad-spectrum immune responses in mice*. *Front Immunol*, 2023. **14**: p. 1142394.
60. Cohen, A.A., et al., *Mosaic RBD nanoparticles protect against challenge by diverse sarbecoviruses in animal models*. *Science*, 2022. **377**(6606): p. eabq0839.
61. Baz, M., et al., *Nonreplicating influenza A virus vaccines confer broad protection against lethal challenge*. *mBio*, 2015. **6**(5): p. e01487-15.
62. Martini, V., et al., *Simultaneous Aerosol and Intramuscular Immunization with Influenza Vaccine Induces Powerful Protective Local T Cell and Systemic Antibody Immune Responses in Pigs*. *J Immunol*, 2021. **206**(3): p. 652-663.
63. Kandasamy, M., et al., *Recombinant single-cycle influenza virus with exchangeable pseudotypes allows repeated immunization to augment anti-tumour immunity with immune checkpoint inhibitors*. *Elife*, 2023. **12**.
64. Yu, J., et al., *DNA vaccine protection against SARS-CoV-2 in rhesus macaques*. *Science*, 2020. **369**(6505): p. 806-811.
65. Chandler, T.L., et al., *Protective mechanisms of nonneutralizing antiviral antibodies*. *PLoS Pathog*, 2023. **19**(10): p. e1011670.
66. Zhang, A., et al., *Beyond neutralization: Fc-dependent antibody effector functions in SARS-CoV-2 infection*. *Nat Rev Immunol*, 2023. **23**(6): p. 381-396.
67. Tang, J. and J. Sun, *Lung tissue-resident memory T cells: the gatekeeper to respiratory viral (re)-infection*. *Curr Opin Immunol*, 2023. **80**: p. 102278.
68. Odle, A., et al., *Tissue-resident memory T cells contribute to protection against heterologous SARS-CoV-2 challenge*. *JCI Insight*, 2024. **9**(23).
69. Zhou, D., et al., *Structural basis for the neutralization of SARS-CoV-2 by an antibody from a convalescent patient*. *Nat Struct Mol Biol*, 2020. **27**(10): p. 950-958.
70. Hsieh, C.L., et al., *Structure-based design of prefusion-stabilized SARS-CoV-2 spikes*. *Science*, 2020. **369**(6510): p. 1501-1505.
71. Crawford, K.H.D., et al., *Protocol and Reagents for Pseudotyping Lentiviral Particles with SARS-CoV-2 Spike Protein for Neutralization Assays*. *Viruses*, 2020. **12**(5).
72. West, A.P., Jr., et al., *Computational analysis of anti-HIV-1 antibody neutralization panel data to identify potential functional epitope residues*. *Proc Natl Acad Sci U S A*, 2013. **110**(26): p. 10598-603.
73. Cohen, A.A., et al., *Mosaic sarbecovirus nanoparticles elicit cross-reactive responses in pre-vaccinated animals*. *Cell*, 2024. **187**(20): p. 5554-5571 e19.

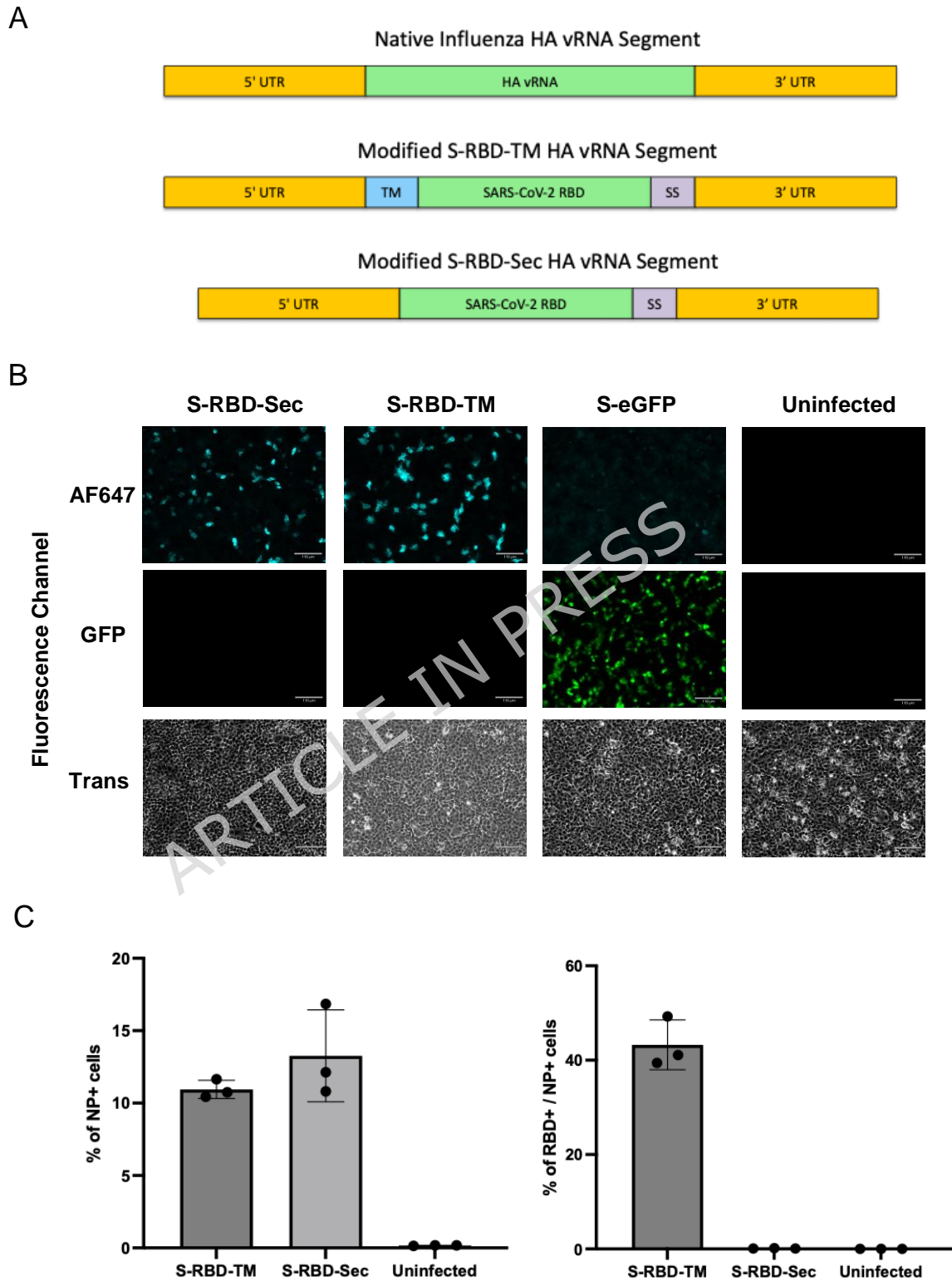
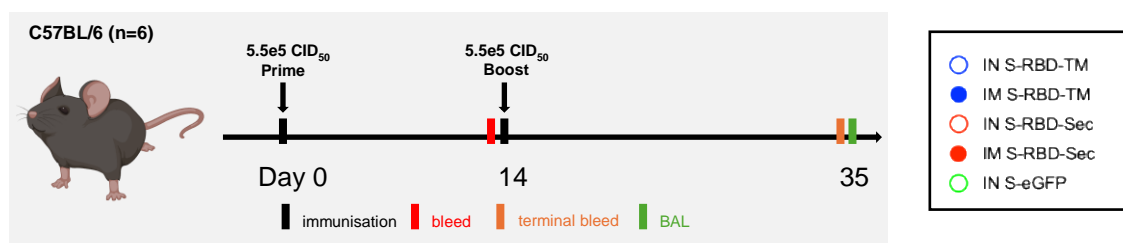


Figure 1: Design and characterisation of S-RBD-Sec and S-RBD-TM. A. Schematic diagram of the native haemagglutinin vRNA, and the modified haemagglutinin vRNA to

encoding the membrane-anchored version of RBD (S-RBD-TM) or secretory RBD (S-RBD-Sec). B. Validation of S-RBD-Sec and S-RBD-TM in cell culture. MDCK cells seeded in 6-well plate were infected with $1e4$ CID_{50} of S-RBD-Sec, S-RBD-TM, S-eGFP (S-Flu expressing GFP) control or remained uninfected. 16 hours post-infection, cells were stained with an RBD-specific IgG1 (EY-6A) followed by a goat anti-human IgG1 labelled with AF647. Cells infected with S-RBD-Sec was permeabilised with 0.5% Triton-X 100 prior to staining. Stained cells were visualised using a fluorescence microscope. C. Proportion of RBD-positive cells among influenza NP-positive cells after infection. MDCK-SIAT1 cells ($n=3$) seeded in 6-well plate were infected with S-RBD-TM, S-RBD-Sec at MOI 0.1, or remained uninfected. 16 hours post infection, cells were stained with RBD-specific IgG1 (EY-6A) labelled with AF488, formalin fixed and permeabilised with 0.5% Triton-X 100, followed by staining with anti-Influenza NP IgG1 (2-8C) labelled with AF647. Cells were then analysed using flow cytometer. Scale bar: 110uM. (UTR: untranslated region, orange boxes: the 3' and 5' packaging sequences of the HA vRNA, SS: signal sequence, TM: transmembrane domain, AF647: Alexa Fluor 647)

ARTICLE IN PRESS

A



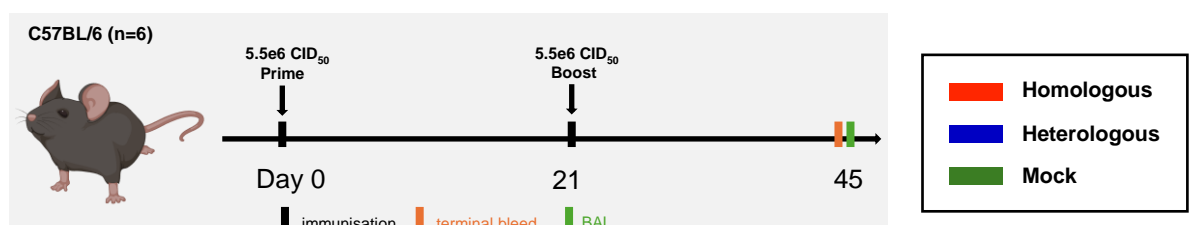
B

C

D

Figure 2: Immunogenicity of S-RBD-TM and S-RBD-Sec in mice. A. Immunisation schedule. Female C57BL/6 mice (n=6) were immunised intranasally or intramuscularly, twice, at Day 0 and Day 14 with either S-RBD-TM or S-RBD-Sec. A mock treated group of mice receiving 2 doses of S-eGFP (S-Flu expressing GFP) was included. Sera was collected on day 13 after prime and 3 weeks after boost. B. Serum antibody binding titre against prototype SARS-CoV-2 Wuhan after prime. C. Serum antibody binding titre against prototype SARS-CoV-2 Wuhan after boost. D. Serum neutralising titre against authentic SARS-CoV-2 Wuhan. The values are presented as geometric mean \pm 95% confident interval. Dotted horizontal line in D represents the lowest sample dilution tested in the assays. Values plotted as 39 in D indicating no detectable binding. Statistical difference was determined using Kruskal-Wallis test followed by Dunn's correction test; *p<0.05, **p<0.01, ***p<0.001. (AUC: area under curve, ID₅₀: half-maximal inhibitory dilution)

A



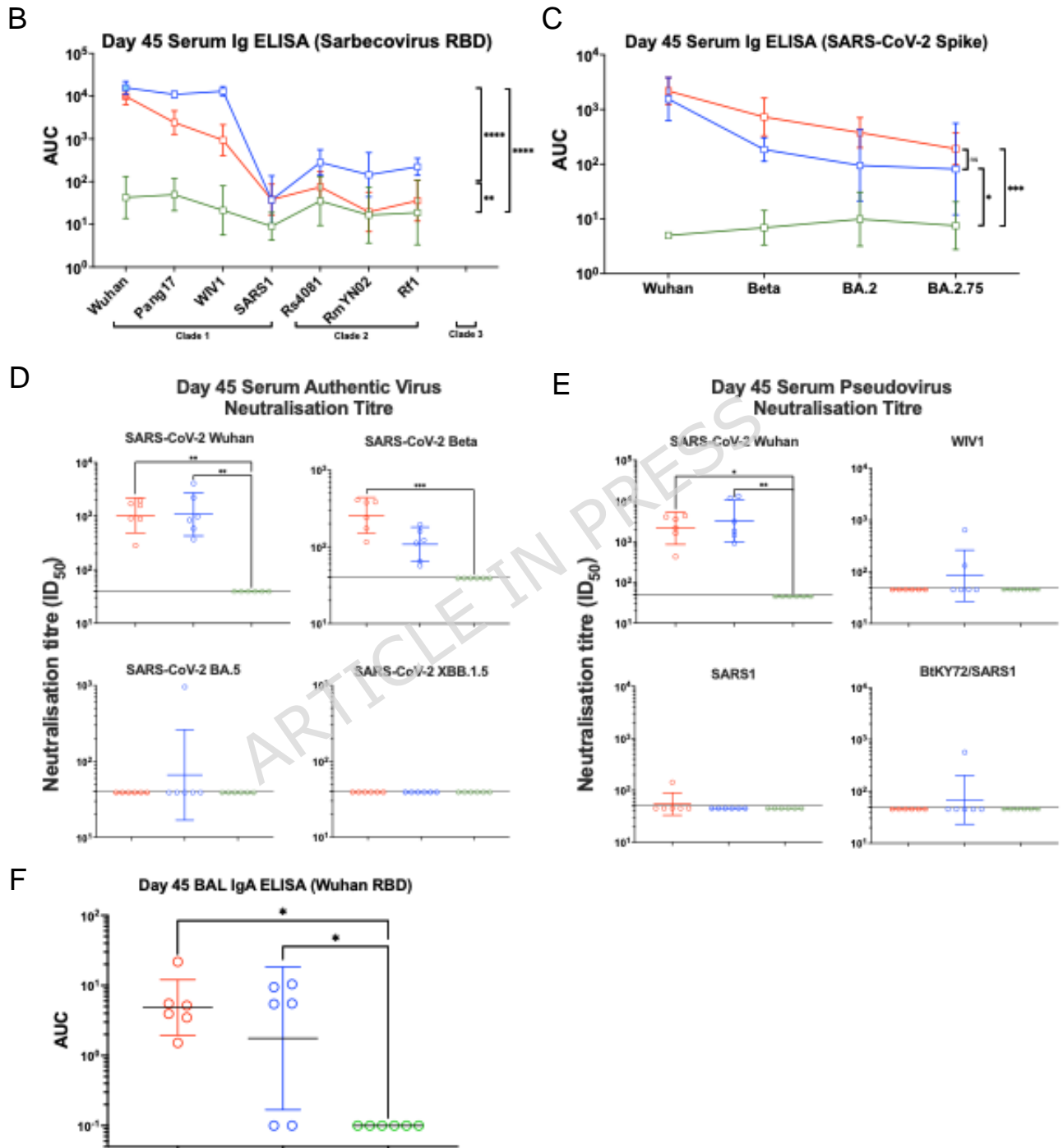


Figure 3: Immunogenicity of homologous and heterologous S-RBD-TM prime-boost in mice. A. Immunisation schedule. Female C57BL/6 mice ($n=6$) were immunised intranasally at Day 0 with S-RBD-TM Wuhan or S-eGFP control (Mock), followed by a boost at Day 21 with

either S-RBD-TM Wuhan (Homologous) or S-RBD-TM BM48-31 (Heterologous). A mock treated group of mice receiving 2 doses of S-eGFP (S-Flu expressing GFP) was included. Sera was collected on day 20 after prime and 3 weeks after boost. Broncho-alveolar lavage (BAL) was collected 3 weeks after boost. B. Serum antibody binding titre against prototype SARS-CoV-2 Variants of Concern (VOCs) Spikes including Wuhan, Beta, BA.2 and BA.2.75. C. Serum antibody binding titre against sarbecovirus RBD (Clade 1 (SARS-CoV-2 Wuhan, Pang 17, WIV1, and SARS1), Clade 2: Rs4081, RmYN02 and Rf1), (Clade 3: BM48-31)). D. Serum neutralisation titre against authentic SARS-CoV-2 VOCs (Wuhan, Beta, BA.4/5, XBB.1.5). E. Serum neutralisation titre against sarbecovirus pseudovirus (Wuhan, WIV1, SARS1 and BtKY72/SARS1 hybrid). F. BAL IgA antibody binding titre against prototype SARS-CoV-2 (Wuhan). The values are presented as geometric mean \pm 95% confident interval. Dotted horizontal lines in D and E represent the lowest serum dilution tested in the assays. Statistical difference in B and C was determined using Tukey's multiple pairwise comparison (means of all RBD tested between immunisation cohorts) followed by the Geisser-Greenhouse correction. Values plotted at 0.1 in F indicating no detectable binding. Statistical difference in D, E and F was determined using Kruskal-Wallis test followed by Dunn's correction test; * $p < 0.05$, ** $p < 0.01$, *** $p < 0.001$, **** $p < 0.0001$. (AUC: area under curve, ID₅₀: half-maximal inhibitory dilution)